Structures of the Neuronal and Endothelial Nitric Oxide Synthase Heme Domain with D-Nitroarginine-Containing Dipeptide Inhibitors Bound†

Mack Flinspach,‡ Huiying Li,‡ Joumana Jamal,‡ Weiping Yang,‡ Hui Huang,§ Richard B. Silverman,§ and Thomas L. Poulos*,‡,||,⊥

Departments of Molecular Biology and Biochemistry, Physiology and Biophysics, and Chemistry and Program in Macromolecular Structure, University of California, Irvine, California 92697-3900, and Department of Chemistry, Department of Biochemistry, Molecular Biology, and Cell Biology and Drug Discovery Program, Northwestern University, Evanston, Illinois 60208-3113

Received December 5, 2003

ABSTRACT: In a continuing effort to unravel the structural basis for isoform-selective inhibition of nitric oxide synthase (NOS) by various inhibitors, we have determined the crystal structures of the nNOS and eNOS heme domain bound with two D-nitroarginine-containing dipeptide inhibitors, D-Lys-D-Arg^{NO_2}-NH_2 and D-Phe-D-Arg^{NO_2}-NH_2. These two dipeptide inhibitors exhibit similar binding modes in the two constitutive NOS isozymes, which is consistent with the similar binding affinities for the two isoforms as determined by K_i measurements. The D-nitroarginine-containing dipeptide inhibitors are not distinguished by the amino acid difference between nNOS and eNOS (Asp 597 and Asn 368, respectively) which is key in controlling isoform selection for nNOS over eNOS observed for the L-nitroarginine-containing dipeptide inhibitors reported previously [Flinspach, M., et al. (2004) *Nat. Struct. Mol. Biol. 11*, 54−59]. The lack of a free α-amino group on the D-nitroarginine moiety makes the dipeptide inhibitor steer away from the amino acid binding pocket near the active site. This allows the inhibitor to extend into the solvent-accessible channel farther away from the active site, which enables the inhibitors to explore new isoform-specific enzyme−inhibitor interactions. This might be the structural basis for why these D-nitroarginine-containing inhibitors are selective for nNOS (or eNOS) over iNOS.

Nitric oxide synthases (NOSs)[1] are a family of enzymes discovered slightly more than a decade ago that catalyze the biosynthesis of NO from L-arginine through two sequential redox reactions using molecular oxygen and electrons provided by NADPH (*1*). Humans and other mammals have three main NOS isoforms: neuronal (nNOS), inducible (iNOS), and endothelial (eNOS). NO produced from nNOS and eNOS serves as a second messenger that triggers signal transduction through the soluble guanylate cyclase/cGMP pathway to exert its physiological functions (*2*, *3*). nNOS-derived NO participates in neurotransmission in both the central and peripheral nerve systems, while eNOS-derived NO is a vasodilator essential for the vascular homeostasis and also inhibits platelet aggregation and leukocyte adhesion. NO produced from iNOS plays an antimicrobial role in host defense (*2*, *3*).

All three NOS isoforms are hemo-flavoenzymes sharing a similar domain architecture (*4*). The N-terminal domain is a heme-containing catalytic module which also binds the essential cofactor, tetrahydrobiopterin (H_4B). The C-terminal domain consists of FMN, FAD, and NADPH binding sites. Only dimeric NOS is catalytically active (*5*), and dimerization occurs through the heme domains (*6*). Binding of calmodulin (CaM) to a linker that connects the heme and flavin domains triggers a little-understood conformational change between the heme and flavin domains which promotes the flow of electrons from the flavins to heme (*7*, *8*). Both eNOS and nNOS activity are regulated by CaM binding, while iNOS contains CaM as a permanently bound subunit; hence, iNOS is regulated at the level of transcription (*9*).

The impaired NO production by eNOS is associated with hypertension (*10*), atherosclerosis (*11*, *12*), and arterial thrombosis (*13*). Excess formation of NO from nNOS has been implicated in stroke (*14*), migraine (*15*), and other neurodegenerative diseases (*16*, *17*). iNOS-produced NO appears to be involved in a broad range of inflammatory pathologies, such as septic shock (*18*, *19*), rheumatoid arthritis (*20*), colitis (*21*), and acute lung inflammation (*22*). Intervention with NOS inhibitors can help alleviate many of these pathological conditions. In general, compounds that control the overproduction of NO by nNOS or iNOS while leaving undisturbed the vasoprotective function of eNOS are desired. Much effort has been devoted in both pharmaceutical

† This research was supported by NIH Grants GM57353 (T.L.P.) and GM49725 (R.B.S.).

* To whom correspondence should be addressed. E-mail: poulos@uci.edu. Telephone: (949) 824-7020. Fax: (949) 824-3280.

‡ Department of Molecular Biology and Biochemistry, University of California.

§ Northwestern University.

|| Department of Physiology and Biophyiscs, University of California.

⊥ Department of Chemistry and Program in Macromolecular Structure, University of California.

[1] Abbreviations: NOS, nitric oxide synthase; nNOS, neuronal NOS; eNOS, endothelial NOS; iNOS, inducible NOS; L-NNA, N^{ω}-nitro-L-arginine; cGMP, cyclic guanidine monophosphate; 2′,5′-ADP, 2′,5′-adenosine diphosphate; NTA, nitrilotriacetic acid.

10.1021/bi0361867 CCC: $27.50
Published on Web 04/14/2004

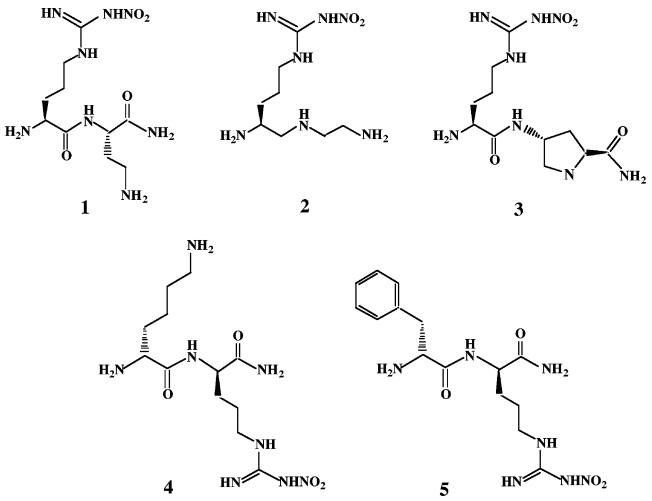

FIGURE 1: Chemical structures and nomenclature of the five dipeptide amide inhibitors in this study: (**1**) L-N^{ω}-nitroarginine 2,4-L-diaminobutyramide, (**2**) (4*S*)-*N*-[4-amino-5-(aminoethyl)amino-pentyl]-*N*′-nitroguanidine, (**3**) L-N^{ω}-nitroarginine-(4*R*)-amino-L-proline amide, (**4**) D-Lys-D-Arg^{NO_2}-NH_2 or D-lysine-D-N^{ω}-nitroarginine amide, and (**5**) D-Phe-D-Arg^{NO_2}-NH_2 or D-phenylalanine-D-N^{ω}-nitroarginine amide.

and academic laboratories to the development of isoform-selective NOS inhibitors (*23*−*25*).

The crystal structures of the dimeric heme domain for all three NOS isoforms now are known (*26*−*29*). Since the heme domain active site is the target for a vast majority of NOS inhibitors, the way is now open for structure-based inhibitor design. Because of the near-identical active site architecture in all three NOS isoforms, it is not surprising that simple L-arginine analogue inhibitors show little isoform selectivity. Nevertheless, certain nitroarginine (NNA)-containing dipeptides have been shown to exhibit excellent isoform selectivity (*30*−*34*). Recently, we determined the crystal structures of nNOS and eNOS complexed with three of these L-NNA-containing dipeptide amide/peptidomimic inhibitors, L-N^{ω}-nitroarginine-2,4-L-diaminobutyramide, (4*S*)-*N*-[4-amino-5-(aminoethyl)aminopentyl]-*N*′-nitroguanidine, and L-N^{ω}-nitroarginine-(4*R*)-amino-L-proline amide, which exhibit ≈1500−2000-fold selectivity for nNOS (and iNOS) over eNOS. An amino acid substitution, Asp 597 in nNOS to Asn 368 in eNOS, was shown to be the major structural basis for isoform selectivity (*35*). Here we report the structures of rat nNOS and bovine eNOS complexed with two D-NNA-containing dipeptide amides, D-Lys-D-Arg^{NO_2}-NH_2 and D-Phe-D-Arg^{NO_2}-NH_2 (Figure 1). These two dipeptides are good inhibitors for either nNOS or eNOS over iNOS. Structures of nNOS and eNOS dipeptide complexes compared with the known iNOS structure provide further insights into the structural basis for isoform selectivity.

EXPERIMENTAL PROCEDURES

Protein Expression and Purification. The pCWori-based NOS plasmids with an N-terminal His_6 tag were provided by P. R. Ortiz de Montellano's laboratory (*36*, *37*). Full-length rat nNOS was expressed in *Escherichia coli* strain BL21(DE3) and purified through 2′,5′-ADP (Amersham) and Ni−NTA (Novegen) columns as described previously (*29*). The heme domain of nNOS was generated by limited trypsinolysis and further purified through a Superdex 200 gel filtration column. The coding sequence of full-length bovine eNOS was excised from the pCWori vector using an *Nde*I−*Xba*I restriction digest and inserted into a pPICZB vector (Invitrogen), which was then used to transform the yeast KM71H Mut^s Pichia strain for protein expression, as described in detail previously (*35*). The 2′,5′-ADP column-purified holo-eNOS was subjected to limited trypsin digestion to obtain the heme domain, which was further purified after passing through a Superdex 200 column.

Crystallization and Diffraction Data Collection. Sitting drop vapor diffusion crystallization conditions for the dipeptide-bound nNOS heme domain are similar to those described for other nNOS−inhibitor complex structures (*29*). Crystal growth conditions for eNOS−dipeptide complexes were the same as those reported previously (*35*).

Freshly grown crystals were passed stepwise through the artificial mother liquor (slight variations in buffer and salt ingredients for nNOS and eNOS) containing an increased amount of cryoprotectants (the final solution comprises 10% glycerol, 10% trehalose, 5% sucrose, and 5% mannitol) prior to the cryogenic X-ray diffraction data collection at ∼100 K. Synchrotron radiation was necessary to bring data to the desired resolution. Diffraction data were recorded with either a Mar Research MAR345 imaging plate at Stanford Synchrotron Radiation Laboratory (SSRL, Palo Alto, CA) or an ADSC CCD Quantum 4 detector at Advanced Light Source (ALS, Berkeley, CA). Observed diffraction data were integrated and scaled with HKL (*38*).

Structure Solution and Refinement. To calculate the initial difference Fourier map, rigid body refinement was usually carried out using CNS (*39*) with a known nNOS or eNOS structure as the starting model omitting substrate and water molecules. Coordinates and temperature factors were further refined to generate the electron density for modeling the dipeptide ligands using the graphics program O (*40*). Water molecules were added with the water picking routine in CNS and visually checked against the electron density. To verify the fit of the inhibitors, toward the end of the refinement, $F_o - F_c$ omit electron density maps were calculated with CNS using the simulated annealing protocol at a starting temperature of 1000 K with the ligand of interest omitted from the calculation (Figure 2). Statistics for data collection and structure refinement are shown in Table 1. Coordinates and structure factors of four inhibitor complex structures reported here have been deposited in the Protein Data Bank as the entries listed in Table 1.

RESULTS AND DISCUSSION

Binding of the Dipeptide to nNOS. For simplicity, inhibitors **1**−**3** (Figure 1) will be termed L-NNA inhibitors, while inhibitors **4** and **5** will be termed D-NNA inhibitors. We recently reported crystal structures of nNOS and eNOS complexed with L-NNA-derived dipeptide inhibitors **1**−**3** (*35*). These dipeptides contain the N-terminal L-NNA whose nitroguanidine group anchors the inhibitor to the NOS substrate binding site through an H-bonding network with surrounding protein groups. Both dipeptide inhibitors studied here, D-Phe-D-Arg^{NO_2}-NH_2 and D-Lys-D-Arg^{NO_2}-NH_2, have the nitroguanidine at the C-terminal end of the dipeptide and the D configuration about Cα (Figure 1). The crystal structures reveal that the nitroguanidine group of C-terminal

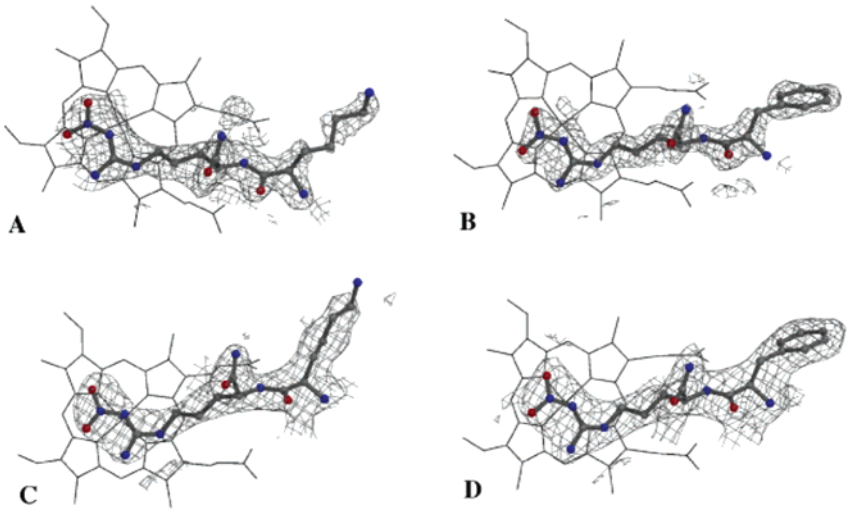

FIGURE 2: $F_o - F_c$ omit maps contoured at 3σ for the D-NNA-containing dipeptides, (A and C) D-Lys-D-Arg^{NO_2}-NH_2 and (B and D) D-Phe-D-Arg^{NO_2}-NH_2, bound in the nNOS and eNOS heme active site, respectively.

Table 1: Data Collection and Refinement Statistics[a]

	nNOS−**4**	nNOS−**5**	eNOS−**4**	eNOS−**5**
cell dimensions (Å)	$a = 51.59$	$a = 52.09$	$a = 57.009$	$a = 58.791$
(space group $P2_12_12_1$)	$b = 109.81$	$b = 110.91$	$b = 106.215$	$b = 106.647$
	$c = 164.67$	$c = 165.03$	$c = 156.536$	$c = 157.659$
PDB Code	1RS6	1RS7	1RS8	1RS9
data resolution (Å)	1.93	1.95	2.30	2.22
total no. of observations	253473	222738	177804	210329
no. of unique reflections	66295	64254	42219	49047
R_{sym}[b]	0.062 (0.709)[c]	0.037 (0.149)[c]	0.078 (0.680)[c]	0.069 (0.450)[c]
$\langle I/\sigma \rangle$	11.2 (2.0)[c]	13.2 (4.9)[c]	17.2 (1.7)[c]	31.4 (3.4)[c]
completeness (%)	92.4 (90.9)[c]	91.5 (54.0)[c]	99.1 (97.1)[c]	99.1 (94.0)[c]
no. of reflections used in refinement	65591	64184	39786	46513
R factor[d]	0.222	0.216	0.222	0.218
R_{free}[e]	0.254	0.251	0.276	0.267
no. of protein atoms	6655	6655	6443	6443
no. of heterogeneous atoms	201	193	195	199
no. of water molecules	550	569	441	376
rms deviation				
bond lengths (Å)	0.010	0.011	0.008	0.008
bond angles (deg)	1.5	1.5	1.5	1.5

[a] nNOS−**4**, nNOS complexed with the dipeptide amide inhibitor D-Lys-D-Arg^{NO_2}-NH_2 (Figure 1); nNOS−**5**, nNOS with D-Phe-D-Arg^{NO_2}-NH_2; eNOS−**4**, eNOS with D-Lys-D-Arg^{NO_2}-NH_2; eNOS−**5**, eNOS with D-Phe-D-Arg^{NO_2}-NH_2. [b] $R_{sym} = \sum|I - \langle I \rangle|/\sum I$, where I is the observed intensity of a reflection and $\langle I \rangle$ the averaged intensity of multiple observations of the reflection and its symmetry mates. [c] The values in parentheses were obtained in the outermost resolution shell. [d] R factor $= \sum||F_o| - |F_c||/\sum|F_o|$, where F_o and F_c are the observed and calculated structure factors, respectively. [e] R_{free} was calculated with the 5% of the reflections set aside randomly throughout the refinement.

D-NNA occupies the same substrate binding site as in L-NNA, an observation which was correctly predicted by a *retro-inverso* binding model and ENDOR spectroscopic measurements (*41*). Therefore, the nitroguanidine group binds in the same fashion to NOS independent of the D or L configuration about Cα or the location of the nitroguanidine group at the C- or N-terminal end of the dipeptide. The nitroguanidine moiety contributes a total of three H-bonds (Figure 3), including two between its guanidino nitrogens and the Glu 592 side chain and one from its nitro group to the backbone amide nitrogen of Gly 586. To satisfy all of the H-bonding interactions, the nitro group of the inhibitor is 5−15° out of the guanidino plane.

The carboxamide group in the D-NNA inhibitors, however, interacts with the protein in a manner different from that in the L-NNA inhibitors. There are two main differences between D-NNA inhibitors and L-NNA inhibitors. First, the carboxamide group is attached to Cα of D-NNA and thus is closer to the heme than in the L-NNA inhibitors where the carboxamide group belongs to the second amino acid. Second, the D configuration at Cα in D-NNA positions the carboxamide group close to surrounding protein groups. As a consequence, Gln 478 and Arg 481 must move to accommodate the carboxamide group of the inhibitor (Figure 3). The side chain of Arg 481 changes its χ_3 torsion angle by 60° which places a guanidino terminal nitrogen in position to H-bond with a carboxamide oxygen of the dipeptide inhibitor. This altered Arg 481 side chain position is stabilized by a new H-bond between the guanidino NE atom of Arg 481 and the amide oxygen of Gln 478. The movement of Arg 481 results in the loss of an H-bond with the OH group of Ser 477 normally observed in most other nNOS structures where either the substrate or other inhibitors are bound (Figure 3).

The peptide amide nitrogen in both D-NNA inhibitors is situated between the two heme propionates and exhibits good H-bonding geometry with one of the propionates (Figure 3). The peptide carbonyl oxygen from the second residue, either

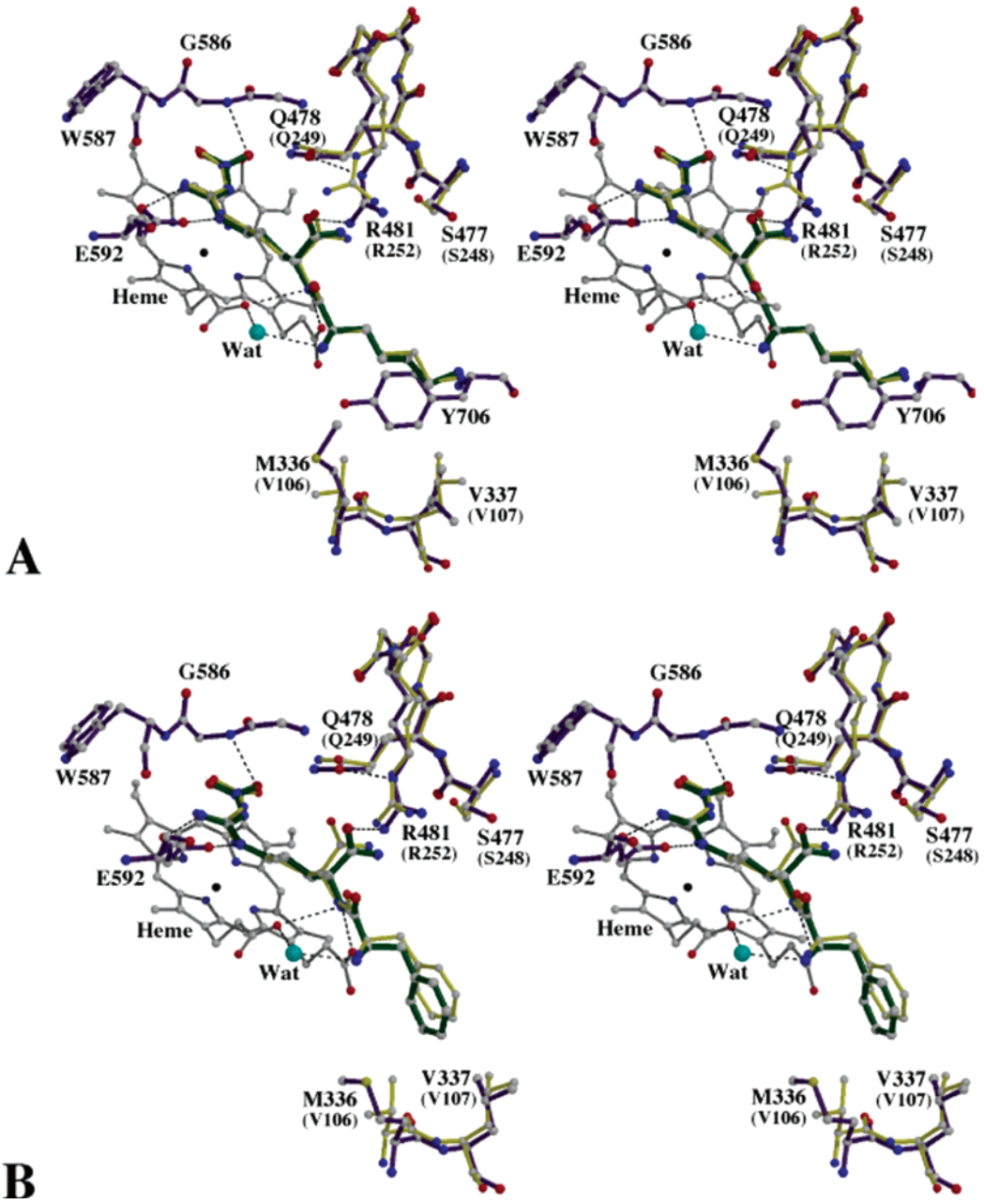

FIGURE 3: Stereoviews of (A) D-Lys-D-Arg^{NO_2}-NH_2 and (B) D-Phe-D-Arg^{NO_2}-NH_2 found at the nNOS and eNOS substrate binding site. Protein residues surrounding the inhibitor are mostly conserved among the two isoforms. Therefore, wherever the protein−inhibitor interactions are identical in both isoforms, only the residues of nNOS are shown and labeled; wherever the differences exist, the residues of nNOS (indigo) and those of eNOS (yellow) are superimposed. Labels for eNOS are in parentheses. Hydrogen bonds are denoted with dashed lines. The protein atom color scheme is as follows: gray for carbon, blue for nitrogen, and red for oxygen.

D-Phe or D-Lys, does not directly contact the protein, whereas the α-amino nitrogen of the second residue forms an H-bonding network with both heme and H_4B through a water molecule that is bridging the heme propionate and the oxygen at the 4-position of the pterin ring (Figure 4).

The only structural difference between these two D-NNA-containing dipeptides lies in the side chain of the second residue, Phe vs Lys. The side chains of both are situated in a pocket (Figure 4) surrounded by Met 336, Leu 337, Tyr 706, and Trp 306 (from the other subunit). To avoid a potential clash with the phenyl ring in D-Phe-D-Arg^{NO_2}-NH_2, the Met 336 side chain adopts a different rotamer which relaxes the contact to more than 4.0 Å. The phenyl ring also contacts Leu 337, Tyr 706, and Trp 306 at distances of less than 4.0 Å (Figure 4). The phenyl plane is almost perpendicular to the aromatic rings of both Tyr 706 and Trp 306, but there is not enough mutual overlap for favorable aromatic interactions. In contrast, the lysine methylene groups in D-Lys-D-Arg^{NO_2}-NH_2 makes closer contact with only the Tyr 706 ring (Figure 3A), while the lysine terminal amino group extends into solvent with no H-bonding or ion pairing interactions with neighboring protein groups.

The structural features revealed by these two nNOS structures also provide an explanation for why D-NNA-containing dipeptides are good NOS inhibitors while D-NNA alone is not. It is well-known that the amino acid binding pocket in the NOS active site only accommodates the amino and carboxylate groups in an L configuration about Cα. A D-amino acid could at best retain one of the two functional groups in the binding pocket, leaving the other one out, which

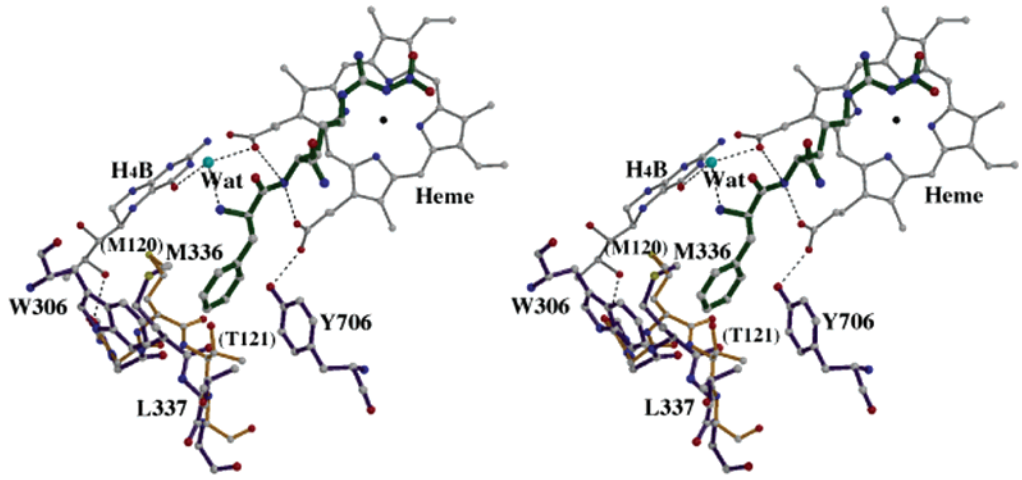

FIGURE 4: Overlay of the D-Phe-D-Arg^{NO_2}-NH$_2$-bound nNOS structure (indigo) onto the human iNOS structure (orange, PDB entry 1NSI). The electrostatically unfavorable contact and steric clashing between the phenyl ring of inhibitor and the Thr 121 side chain in iNOS might explain this inhibitor's poor affinity (millimolar) for the isoform.

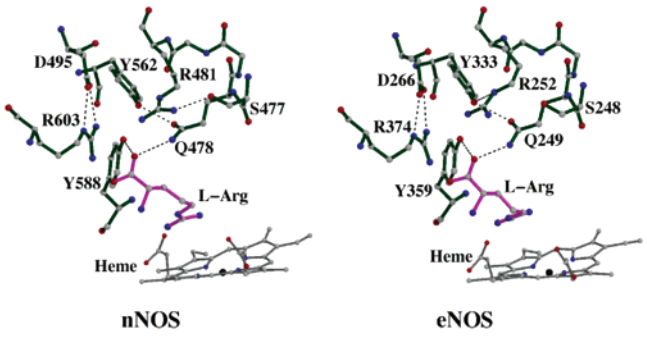

FIGURE 5: Comparison of the nNOS and eNOS active site with the substrate bound. The hydrogen bonding (dashed lines) pattern is identical for Arg 603 of nNOS and Arg 354 of eNOS, but quite different for Arg 481 of nNOS and Arg 252 of eNOS.

would substantially reduce the affinity for the NOS active site. The D-NNA-containing dipeptides described here, however, have steered away from the amino acid binding pocket. This allows the D-NNA-containing dipeptides to explore new interactions with the surrounding protein, either H-bonding or van der Waals contacts, in the broad solvent-accessible channel via the carboxamide group of NNA as well as other functional groups in the second amino acid moiety. It thus appears that the additional new interactions afforded by the larger dipeptide and its associated functional groups make the configuration about Cα far less important for binding.

Binding of the Dipeptide to eNOS. The two D-NNA-containing dipeptides bind to eNOS (Figure 3) in the same mode as what was just described for nNOS which explains why these inhibitors bind with similar affinities to both nNOS and eNOS. Nevertheless, there are subtle structural differences between isoforms. One is the triad interactions between the carboxamide of D-NNA, Gln 249, and Arg 252 (Gln 478 and Arg 481, respectively, in nNOS). When substrate-bound structures of both eNOS and nNOS are compared, residue Arg 252 in eNOS adopts a side chain conformation different from that of Arg 481 in nNOS. Instead of H-bonding with the neighboring Ser 248 as observed between Arg 481 and Ser 477 in nNOS, Arg 252 in eNOS forms an H-bond with Tyr 333 (Figure 5). The side chain conformation of Arg 252 in eNOS is less extended than that of Arg 481 in nNOS. Consequently, when either D-NNA inhibitor binds, the impact on the position of this Arg is weaker in eNOS than in nNOS. Arg 252 in eNOS does lose its H-bond to Tyr 333, but does not interact with the carboxamide in D-Lys-D-Arg^{NO_2}-NH$_2$ (Figure 3A) or only forms a loose contact with carboxamide in D-Phe-D-Arg^{NO_2}-NH$_2$ (Figure 3B). Gln 249 in eNOS, like Gln 478 in nNOS, rotates to make an H-bond to both the carboxamide of D-nitroarginine-NH$_2$ and the guanidino NE atom of Arg 252. Another subtle difference is that the Ser 248 side chain rotamer in eNOS is not affected by this movement of Arg 252.

The second enzyme−inhibitor contact point where there is a difference between nNOS and eNOS results from an amino acid substitution: Met 336 in nNOS versus Val 106 in eNOS. The shorter side chain of Val 106 leaves a void next to H$_4$B, which has been filled by a glycerol molecule in the eNOS crystal structures. Interestingly, the wider branched side chain of Val 106 results in closer contacts with the phenyl ring of D-Phe-D-Arg^{NO_2}-NH$_2$, pushing it away slightly relative to the phenyl ring position observed in the nNOS structure (Figure 3B). In the D-Lys-D-Arg^{NO_2}-NH$_2$ structure, Val 106 is too far from the lysine tail for direct contact (Figure 3A). Similar to the situation in nNOS, the phenyl ring in D-Phe-D-Arg^{NO_2}-NH$_2$ exhibits more favorable nonbonded interactions (<4.0 Å) than the lysine tail in D-Lys-D-Arg^{NO_2}-NH$_2$ does to the surrounding residues, Val 106, Leu 107, Tyr 477, and Trp 76 (the other subunit). However, this structural difference creates little difference in the overall binding affinity since D-Phe-D-Arg^{NO_2}-NH$_2$ binds with K_i values of 2 and 5 μM for nNOS and eNOS, respectively (*31*), while D-Lys-D-Arg^{NO_2}-NH$_2$ binds to nNOS with a K_i of 0.89 μM compared to a K_i of 30 μM for eNOS.

In sharp contrast to the similar inhibitory potency of the D-NNA inhibitors, the L-NNA inhibitors are 1500−2000-fold more selective for nNOS than for eNOS (*31*, *33*). The key to why L-NNA inhibitors are selective is primarily a single amino acid difference: Asn 368 in eNOS versus Asp 597 in nNOS (*35*). In L-NNA inhibitors, the free α-amino group of NNA is situated between Asp 597 and Glu 592. As a result, Asp 597 provides greater electrostatic stabilization of the L-NNA α-amino group that Asn 368 in eNOS fails to offer. In the D-NNA inhibitors, however, the α-amino

group of NNA is part of the peptide bond while the free α-amino group of the second residue is located much farther from Asn 368 or Asp 597. This indicates that the model originally proposed for how these *retro-inverso* dipeptide amides bind to the active site is correct in predicting the binding of nitroguanidine next to heme, but incorrect in predicting that the α-amino group of both L- and D-dipeptides can interact with the same active site carboxylate (*41*). Hence, the D-NNA inhibitors are not distinguished by this single residue difference between eNOS and nNOS. These studies with D-NNA inhibitors therefore support our earlier hypothesis (*35*) that a single amino acid difference between eNOS and nNOS is the primary factor controlling isoform selectivity with L-NNA inhibitors.

Postulated Structural Basis for Isoform Selection over iNOS. Although the two D-NNA-containing dipeptides bind very similarly to both eNOS and nNOS, which explains their similar inhibitory potency (*31*), both D-NNA dipeptides are very poor inhibitors of murine iNOS, the K_i values being 910 and 3600 μM for D-Lys-D-Arg^{NO_2}-NH_2 and D-Phe-D-Arg^{NO_2}-NH_2, respectively. Such a low affinity for iNOS has prevented cocrystallization of the D-NNA inhibitors with iNOS. As a result, we turned to molecular modeling to provide some insight into isoform selectivity by overlaying the structures of murine or human iNOS onto that of the nNOS dipeptide complex. One possible contributor to D-NNA dipeptide selectivity is Asn 115 in murine iNOS (Thr 121 in human iNOS) which replaces Leu 337 in nNOS (or Leu 107 in eNOS). As described earlier, the Phe and Lys side chains of the D-NNA inhibitors form hydrophobic nonbonded contacts with Leu 337 in nNOS (Figure 3). Hence, a polar side chain at this location is unlikely to provide favorable nonbonded interactions. Steric crowding between the D-NNA inhibitors and Asn 115 in murine iNOS (Thr 121 in human iNOS) is another possible factor. Asn 115 (or Thr 121) resides at the N-terminal end of a loop that connects the Zn center with the first helix in the iNOS structure, a loop that is well-ordered in iNOS but is highly disordered in both eNOS and nNOS structures. Still, the N-terminus of the loop is visible in all three structures and reveals that Asn 115 (or Thr 121) in iNOS is closer to the active site than Leu 337 in nNOS (Leu 107 in eNOS), resulting in a narrower substrate access channel in iNOS (Figure 4). The side chain of Phe or Lys of the D-NNA dipeptide inhibitors may sterically clash with Asn 115 (Thr 121) in iNOS and may explain their low affinity for this isoform.

The region that interacts with the carboxamide of D-NNA inhibitors might also contribute to their isoform selection for constitutive NOS over iNOS. As described earlier, although there is no amino acid substitution in this region, significant side chain flexibility has been observed for Arg 481 in nNOS and Arg 252 in eNOS. We would expect similar flexibility for Arg 260 in murine iNOS (or Arg 266 in human iNOS), especially since different side chain conformations have been observed for this Arg residue in structures of all NOS isoforms. There are a few other Arg residues lining the inner surface of the substrate access channel, for instance, Arg 603 in nNOS or Arg 374 in eNOS (Figure 5), whose side chain conformation varies little from one isoform to another because of tight salt bridges with a neighboring acidic residue. In contrast, Arg 481 in nNOS or its counterpart in other isoforms does not have an acidic residue nearby. Instead, this Arg forms an H-bond with a neighboring residue, Tyr in eNOS and Ser in nNOS. Interestingly, the corresponding Arg 128 in *Bacillus subtilis* NOS (*42*) H-bonds directly to the carboxylate of the substrate, L-Arg. The conformational variability of this Arg and its local environment enables this Arg to closely contact the D-NNA inhibitors in nNOS with somewhat looser contacts in eNOS. We speculate that in combination with the narrower active site channel in iNOS, this Arg may not form close contacts with D-NNA inhibitors which would further contribute to the observed high K_i values for these two D-NNA dipeptides with iNOS compared to those with nNOS and eNOS.

In summary, crystal structures of the nNOS and eNOS heme domain bound to D-NNA-containing dipeptides, D-Phe-D-Arg^{NO_2}-NH_2 or D-Lys-D-Arg^{NO_2}-NH_2, have revealed a similar binding mode for the two inhibitors for the two constitutive isoforms. This is consistent with their similar inhibitory potency toward constitutive NOS observed in the K_i measurements. Lacking a free α-amino group on the NNA moiety makes these two dipeptide inhibitors insensitive to the amino acid difference between nNOS and eNOS (Asp 597 and Asn 368, respectively). We postulate that the structural basis for the selectivity of the two inhibitors against iNOS stems primarily from the specific enzyme−inhibitor interactions around the side chain of the second residue within the dipeptide.

ACKNOWLEDGMENT

We thank the beamline staff at SSRL and ALS for their assistance during synchrotron data collection.

REFERENCES

1. Griffith, O. W., and Stuehr, D. J. (1995) *Annu. Rev. Physiol. 57*, 707−736.
2. Moncada, S., Palmer, R. M. J., and Higgs, E. A. (1991) *Pharmacol. Rev. 43*, 109−142.
3. Kerwin, J. F., Jr., Lancaster, J. R., Jr., and Feldman, P. L. (1995) *J. Med. Chem. 38*, 4343−4362.
4. Masters, B. S., McMillan, K., Sheta, E. A., Nishimura, J. S., Roman, L. J., and Martasek, P. (1996) *FASEB J. 10*, 552−558.
5. Baek, K. J., Thiel, B. A., Lucas, S., and Stuehr, D. J. (1993) *J. Biol. Chem. 268*, 21120−21129.
6. Siddhanta, U., Presta, A., Fan, B., Wolan, D., Rousseau, D. L., and Stuehr, D. J. (1998) *J. Biol. Chem. 273*, 18950−18958.
7. Abu-Soud, H. M., and Stuehr, D. J. (1993) *Proc. Natl. Acad. Sci. U.S.A. 90*, 10769−10772.
8. Roman, L. J., Martasek, P., and Masters, B. S. S. (2002) *Chem. Rev. 102*, 1179−1189.
9. Nathan, C., and Xie, Q. (1994) *J. Biol. Chem. 269*, 13725−13728.
10. Taddei, S., Virdis, A., Ghiadoni, L., Sudano, I., and Salvetti, A. (2001) *J. Cardiovasc. Pharmacol. 38* (Suppl. 2), S11−S14.
11. Sachais, B. S. (2001) *Curr. Atheroscler. Rep. 3*, 412−416.
12. Rekka, E. A., and Chrysselis, N. C. (2002) *Mini Rev. Med. Chem. 2*, 433−445.
13. Loscalzo, J. (2001) *Circ. Res. 88*, 756−762.
14. Sims, N. R., and Anderson, M. F. (2002) *Neurochem. Int. 40*, 511−526.
15. Iversen, H. K. (2001) *Cephalagia 21*, 781−785.
16. Dawson, V. L., and Dawson, T. M. (1998) *Prog. Brain Res. 118*, 215−229.
17. Calabrese, V., Bates, T. E., and Stella, A. M. (2000) *Neurochem. Res. 25*, 1315−1341.
18. Brealey, D., Brand, M., Hargreaves, I., Heales, S., Land, J., Smolenski, R., Davies, N. A., Cooper, C. E., and Singer, M. (2002) *Lancet 360*, 219−223.

19. Boveris, A., Alvarez, S., and Navarro, A. (2002) *Free Radical Biol. Med. 33*, 1186−1193.
20. Bingham, C. O., III (2002) *J. Rheumatol. Suppl. 65*, 3−9.
21. Cho, C. H. (2001) *J. Physiol. Paris 95*, 253−256.
22. Shanley, T. P., Zhao, B., Macariola, D. R., Denenberg, A., Salzman, A. L., and Ward, P. A. (2002) *Crit. Care Med. 30*, 2143−2145.
23. Southan, G. J., and Szabo, C. (1996) *Biochem. Pharmacol. 51*, 383−394.
24. Babu, B. R., and Griffith, O. W. (1998) *Curr. Opin. Chem. Biol. 2*, 491−500.
25. Alberton, W. K., Cooper, C. E., and Knowles, R. G. (2001) *Biochem. J. 357*, 593−615.
26. Crane, B. R., Arvai, A. S., Ghosh, D. K., Wu, C., Getzoff, E. D., Stuehr, D. J., and Tainer, J. A. (1998) *Science 279*, 2121−2126.
27. Raman, C. S., Li, H., Martasek, P., Kral, V., Masters, B. S., and Poulos, T. L. (1998) *Cell 95*, 939−950.
28. Fischmann, T. O., Hruza, A., Niu, X. D., Fossetta, J. D., Lunn, C. A., Dolphin, E., Prongay, A. J., Reichert, P., Lundell, D. J., Narula, S. K., and Weber, P. C. (1999) *Nat. Struct. Biol. 6*, 233−242.
29. Li, H., Shimizu, H., Flinspach, M., Jamal, J., Yang, W., Xian, M., Cai, T., Wen, E. Z., Jia, Q., Wang, P. G., and Poulos, T. L. (2002) *Biochemistry 41*, 13868−13875.
30. Silverman, R. B., Huang, H., Marletta, M. A., and Martasek, P. (1997) *J. Med. Chem. 40*, 2813−2817.
31. Huang, H., Martasek, P., Roman, L. J., Masters, B. S., and Silverman, R. B. (1999) *J. Med. Chem. 42*, 3147−3153.
32. Huang, H., Martasek, P., Roman, L. J., and Silverman, R. B. (2000) *J. Med. Chem. 43*, 2938−2945.
33. Hah, J.-M., Roman, L. J., Martasek, P., and Silverman, R. B. (2001) *J. Med. Chem. 44*, 2667−2670.
34. Hah, J.-M., Roman, L. J., Martasek, P., and Silverman, R. B. (2001) *J. Med. Chem. 44*, 2667−2675.
35. Flinspach, M. L., Li, H., Jamal, J., Yang, W., Huang, H., Hah, J.-M., Gomez-Vidal, J. A., Litzinger, E. A., Silverman, R. B., and Poulos, T. L. (2004) *Nat. Struct. Mol. Biol. 11*, 54−59.
36. Gerber, N. C., and Ortiz de Montellano, P. R. (1995) *J. Biol. Chem. 270*, 17791−17796.
37. Rodriguez-Crespo, I., Gerber, N. C., and Ortiz de Montellano, P. R. (1996) *J. Biol. Chem. 271*, 11462−11467.
38. Otwinowski, Z., and Minor, W. (1997) *Methods Enzymol. 276*, 307−326.
39. Brunger, A. T., Adams, P. D., Clore, G. M., DeLano, W. L., Gros, P., Grosse-Kunstleve, R. W., Jiang, J.-S., Kuszewski, J., Nilges, M., Pannu, N. S., Read, R. J., Rice, L. M., Simonson, T., and Warren, G. L. (1998) *Acta Crystallogr. D54*, 905−921.
40. Jones, T. A., Zou, J.-Y., Cowan, S. W., and Kjeldgaarrd, M. (1991) *Acta Crystallogr. A47*, 110−119.
41. Tierney, D. L., Huang, H., Martasek, P., Roman, L. J., Silverman, R. B., and Hoffman, B. M. (2000) *J. Am. Chem. Soc. 122*, 7869−7875.
42. Pant, K., Bilwes, A. M., Adak, S., Stuehr, D. J., and Crane, B. R. (2002) *Biochemistry 41*, 11071−11079.

BI0361867